



# Study of Droplet Impact on a Wall using a Sharp Interface Method and Different Contact Line Models

M. Emdadi and P. Pournaderi <sup>†</sup>

*Department of Mechanical Engineering, Yasouj University, Yasouj, Iran*

<sup>†</sup>Corresponding Author Email: [sp.pournaderi@yu.ac.ir](mailto:sp.pournaderi@yu.ac.ir)

(Received March 19, 2018; accepted December 2, 2018)

## ABSTRACT

In this research, droplet impact on a surface is simulated by using a sharp method for interface modeling. The level-set method along with the ghost fluid method is used to model interface in a sharp fashion. Different contact line models are compared and evaluated at both low and high impact velocities. On a hydrophobic surface, dynamic models developed by Hoffman and Jiang represent a more accurate prediction of droplet behavior during the impact process than the static and molecular kinetic dynamic models, especially at rebounding stage. At lower impact velocities, the Hoffman's model represents better predictions. However, at higher impact velocities, the Jiang's model is somewhat more accurate. The molecular dynamic model is not appropriate for high impact velocities. On a hydrophilic surface, at low impact velocities, the Jiang's model represents satisfactory results, whereas the static and the Hoffman's models cannot produce accurate results, after initial stages of the impact process. At high impact velocities, the static model shows considerable deviation from the experimental results. The effect of the contact angle on the dynamic behavior of the droplet is investigated. At contact angles lower than  $90^\circ$ , the droplet only spreads on the surface after impact. However, at contact angles higher than  $90^\circ$ , the droplet starts to recoil after spreading. In this case, it is possible that droplet rebounds from surface after recoiling. Maximum spreading radius of the droplet decreases by an increase in contact angle. At higher contact angles, less time is needed for the droplet to rebound from surface.

**Keywords:** Droplet impact; Dynamic contact angle; Level-set method; Ghost fluid method.

## NOMENCLATURE

$D_0$	droplet initial diameter	$\Gamma$	interface
$g$	gravity vector	$\theta$	contact angle
$n$	unit normal vector	$\kappa$	curvature
$p$	pressure	$\mu$	viscosity
$R_0$	droplet initial radius	$\tau$	viscous stress tensor
$t$	unit tangent vector	$\phi$	level-set function
$t$	time	$\nabla$	gradient operator
$u$	velocity vector	$\sigma$	surface tension
$V_0$	droplet initial velocity	<b>Subscripts</b>	
$We$	weber number	$d$	dynamic
		$e$	equilibrium
		$g$	gas
$\rho$	density	$l$	liquid
		$w$	wall

## 1. INTRODUCTION

Liquid jets have a wide application in industry. Droplets produced after liquid jetting may impact

on solid surfaces. During their impact on a surface droplets exhibit different behaviors which are dependent on their physical properties such as viscosity, density and surface tension. Droplet

diameter, impact velocity and solid surface properties such as surface roughness and contact angle are also important (Sikalo *et al.*, 2006). The amount of the wettability of a surface is determined by the contact angle between the droplet and solid surface. This angle, as it is observed in Fig. 1, is formed between the droplet and the surface at the interface of solid, liquid and gas phases. Existence of interface is due to particular energy called surface free energy which is proportional to the number of molecules at interface. In the droplet spreading phenomenon, there is an interface among three different phases (solid, liquid and gas). Thus, there are three kinds of surface energies (per unit surface): liquid/gas  $\gamma_{lg}$ , solid/gas  $\gamma_{sg}$ , solid/liquid  $\gamma_{sl}$ . Due to the amount of these energies, an equilibrium contact angle (i.e., Young angle) is formed between the droplet and the surface. For a smooth and chemically homogenous surface, this angle is expressed as (Zisman *et al.*, 1964),

$$\cos(\theta) = \frac{\gamma_{sg} - \gamma_{sl}}{\gamma_{lg}} \quad (1)$$

Initial studies on the droplet impact problem were initiated by Worthington (1877) who examined water, milk and mercury droplet impact on glass surfaces. Following that, many experimental and theoretical studies were conducted into this problem. In the first numerical models, the effect of surface tension and contact angle were neglected (Harlow and Shannon, 1967). In the models developed later, a constant contact angle was considered (Tsurutani *et al.*, 1990). These models were more accurate than initial models.

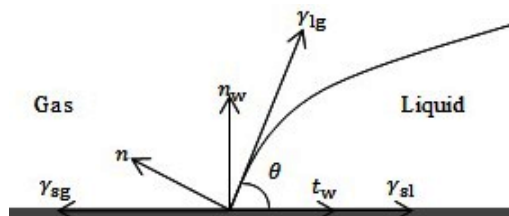


Fig. 1. Contact angle between droplet and surface.

Pasandideh-Fard *et al.* (1996) investigated the droplet impingement on a wall both experimentally and numerically. The interface was captured by using the volume of fluid method. They measured the contact angles at different times during the impact process and used these values in their simulations. They added a surfactant to the droplet liquid and observed no significant effect in the initial stages of the impact process. However, maximum spreading radius and recoil height decreased. Bussmann *et al.* (2000) studied droplet impact on a surface at high impact velocities both experimentally and numerically. They used average contact angle observed in their experiments for simulation. They also used linear volume tracking algorithm for interface capturing. At high impact velocities, after initial spreading, droplet breaks up and a number of small droplets are formed.

Enhancement of contact angle in the spreading stage enhances the number of these small droplets after break-up. Kim *et al.* (2001) studied droplet collision with a surface both experimentally and analytically. They focused on the recoiling stage of the impact process. They found that the droplet recoils faster when Ohnesorge number decreases or Weber number increases. In addition, droplets with higher equilibrium contact angles recoil faster. They reported that Ohnesorge number has the most important role in the recoiling stage. Liu *et al.* (2005) simulated the droplet impingement on a solid surface with an arbitrary shape. They employed a sharp interface method for solid immersed boundaries. They modeled the liquid-liquid interface in a sharp fashion by using a combination of the level-set and ghost fluid methods. They applied constant advancing and receding contact angles in their simulations. The results were validated against the experimental method. Afkhami and Bussmann (2006) studied the collision of the droplet on an inclined surface by using the volume of fluid method. They utilized three simple contact line models. These models were based on the values of the advancing and receding contact angles. The difference among these models was the way in which advancing and receding values were connected at small contact line velocities. They concluded that a small difference in contact angle models can lead to different deformations of the droplet during the impact process. Gatne (2006) studied droplet collision with hydrophilic and hydrophobic surfaces. The nature of surface has an important role in the creation of different regimes. Moreover, changes in viscosity and surface tension affect droplet behavior considerably. Reduction of surface tension results in further wetting of the surface. A similar effect is observed when viscosity is reduced. Fujimoto *et al.* (2007) modeled droplet impact on inclined surfaces by using dynamic contact angle. They employed the VOF method for interface capturing. Droplet spreading radius is enhanced by enhancement of surface inclination and is decreased by an increase in viscosity. Lunkad *et al.* (2007) simulated the droplet impact process on a horizontal and inclined surface by using the volume of fluid method. They examined both static and dynamic contact line models. They used the available experimental data for time variations of contact angle to model the contact line dynamically. They found that by using the static model, the impact process on hydrophobic surfaces can be simulated successfully. However, for hydrophilic surfaces, a dynamic model is needed for accurate prediction of the droplet behavior. Roisman *et al.* (2008) developed a new algorithm to model dynamic contact angle. They considered contact angle as a function of instantaneous velocity of contact line. They used the VOF method for interface tracking and successfully modeled impacts with low Weber numbers. Yokoi *et al.* (2009) developed a dynamic contact angle model and subsequently studied the effect of dynamic contact angle on the droplet impact process. They used the volume of fluid method for interface tracking. They compared the

simplified and the precise dynamic contact line models and concluded that precise modeling of dynamic contact angle has a basic role in accurate simulation of the impact process. Afkhami *et al.* (2009) showed that some of the numerical solutions related to droplet-wall interaction are dependent on the mesh spacing. Therefore, they presented a mesh-dependent dynamic contact angle model to solve this problem. They employed the volume of fluid method and successfully simulated the stationary droplet spreading on a surface at low Reynolds and Capillary numbers. Muradoglu and Tasoglu (2010) simulated axisymmetric droplet impact on a surface by using the front tracking method. They concluded that increasing the Weber number increases the maximum spreading radius and droplet equilibrium time after impact. In addition, increasing the Reynolds number increases the droplet spreading radius. However, for Reynolds numbers higher than 60, the rate of droplet spreading increase is reduced. Sprittles and Shikhmurzaev (2012) proposed a numerical procedure based on the finite element method for the simulation of dynamic wetting phenomenon. They reported that wettability of the surface has an intense effect on the droplet's hydrodynamic behavior. Based on this characteristic, they concluded that chemically patterned surfaces can be designed to obtain different final shapes for the droplet by slightly changing the collision velocity. Bokil (2013) simulated droplet impingement on a wall by using the volume of fluid method. They employed static and dynamic models in their simulations. The results of the static and dynamic models were in good agreement with the experimental results. They reported that the static model represents more accurate prediction of droplet spreading at contact angles higher than 90°. Malgarinos *et al.* (2014) presented a new method for dynamic contact angle modeling. In this method, contact angle is computed based on equilibrium among different forces at contact line. Contact angle effect is considered as a pseudo-adhesion force and is applied in the momentum equation as a source term. The results are satisfactory for low Weber numbers ( $We < 80$ ) and in the spreading stage. Griebel and Klitz (2014) presented a three-dimensional simulation of droplet impact on a surface based on the dynamic contact line models developed by Yokoi *et al.* (2009) and Shikhmurzaev *et al.* (2008). To accomplish this, the smeared-out formulation of the level-set method was utilized for interface capturing. Good agreement was observed with the experimental results for both contact line models. They evaluated the global and local volume correction methods during the impact process and concluded that both methods produce satisfactory results. They pointed out that applying the contact line condition based on the distance function property of the level-set function may produce inaccurate results. This is because the distance function property of the level-set function is not always fulfilled during the solution procedure. They modified the contact line condition to overcome this problem. Hu *et al.* (2015) simulated droplet impingement on a wax

surface. They used the phase-field method for interface tracking. They considered the effect of initial inertia force and contact angle on the droplet behavior during the impact process. In the spreading stage, initial inertia force has more effect on the droplet behavior than contact angle. However, the effect of contact angle is more considerable in the recoiling and rebounding stages. Luo *et al.* (2015) developed a conservative sharp interface approach based on the weakly compressible model for the simulation of incompressible multiphase flows. A curvature boundary condition was imposed for modeling droplet impact on a surface (Luo *et al.*, 2016). By using the presented method, they successfully simulated the spreading of a stationary droplet on a surface. Zhang *et al.* (2016) used the phase-field method and the static contact angle model to simulate droplet collision with a surface. They reported that high viscosity and surface tension reduce the spreading radius of the droplet on the surface. In addition, droplet rebounding occurs only on hydrophobic surfaces. Raman *et al.* (2016) evaluated the effect of the surface inhomogeneity on the droplet behavior during the impact process. The surface inhomogeneity changes the wettability characteristics of the surface by creating wettability gradient on the surface. On a surface with a high constant wettability gradient, after spreading stage, intense recoiling of the upstream end of the droplet occurs. This is followed by the secondary spreading of the downstream end. Guo *et al.* (2016) employed the moment of fluid method to simulate droplet collision on a wall. They simulated the droplet deposition on a hydrophilic wall by using both static and dynamic contact line models. The dynamic models of Kistler *et al.* (1993), Jiang *et al.* (1979) and Yokoi *et al.* (2009) were compared in the droplet deposition process and it was concluded that Jiang *et al.*'s model represents more accurate results. The effect of the surrounding gas on the splash phenomenon on dry and wet surfaces was also studied. For the droplet impact on a dry wall, the splash phenomenon is attenuated by lowering the surrounding gas density. However, on a wet surface, no considerable effect is observed. Vontas *et al.* (2017) compared the static model and the dynamic model developed by Kistler *et al.* (1993). The interface was captured by using the volume of fluid method. They found that the dynamic model reproduces the droplet shape at the spreading and recoiling stages quite successfully. However, the predictions of the static model are only accurate in the spreading stage where the inertia force is dominant. Cimpeanu and Papageorgiou (2018) simulated the oblique impact of a droplet on a surface at high impact velocities by using the volume of fluid method. At high impact velocities, the droplet disintegrates into small droplets after initial spreading. They adopted the static contact angle model for its accuracy in the spreading stage. For impact angles less than 30°, liquid filaments are formed which are detached from the surface near the advancing front of the droplet and are broken up into large droplets. At higher impact angles, the surface tension prevents the droplet breakup.

The literature was reviewed with a focus on the way in which the contact line is modeled. In the previous studies, often a dynamic contact line model was compared with the static model. It is important to know the capability of different contact line models in accurate simulation of the impact process at different impact conditions. As it was observed, the comparative studies on different contact line models are very limited. In the current study, several contact line models are compared and evaluated for low and high impact velocities and different wetting conditions. Impact velocities are in the range in which droplet breakup does not occur.

Previous studies were mainly based on smearing discontinuous quantities across the interface. Kang *et al.* (2000) developed a sharp method for interface modeling by using a combination of the level-set and ghost fluid methods. There are very few studies carried out into the droplet impingement on a solid surface based on the sharp modeling of the interface. In this research, droplet impact on a wall is modeled by using the level-set and ghost fluid methods. Therefore, discontinuity of different variables is preserved across the interface.

## 2. EQUATIONS

### 2.1 Flow Equations

For incompressible and viscous flow, governing equations including momentum and continuity equations are expressed as:

$$\frac{\partial \mathbf{u}}{\partial t} + (\mathbf{u} \cdot \nabla) \mathbf{u} = -\frac{1}{\rho} \nabla p + \frac{1}{\rho} (\nabla \cdot \boldsymbol{\tau})^T + \mathbf{g} \quad (1)$$

$$\nabla \cdot \mathbf{u} = 0 \quad (2)$$

where  $\mathbf{u}$ ,  $\mathbf{g}$ ,  $\rho$ ,  $p$ ,  $t$  and are velocity vector, gravity vector, density, pressure and time, respectively.  $T$  is transpose operator and  $\boldsymbol{\tau}$  is viscous stress tensor which is expressed as:

$$\boldsymbol{\tau} = \mu(\nabla \mathbf{u} + \nabla \mathbf{u}^T) \quad (3)$$

In the above equation  $\mu$  is dynamic viscosity.

### 2.2 Jump Conditions at Interface

The jump in quantity  $A$  across the interface  $\Gamma$  is defined as:

$$[A]_{\Gamma} = A_g - A_l \quad (4)$$

Where  $A_g$  and  $A_l$  are the values of  $A$  in gas and liquid phases, respectively.  $[\cdot]_{\Gamma}$  stands for the jump in quantity  $(\cdot)$  at interface  $\Gamma$ .

Based on the momentum conservation, jump condition at interface can be written as (Kang *et al.*, 2000):

$$\left[ p - 2\mu \mathbf{m} \cdot \nabla \mathbf{u} \cdot \mathbf{n}^T \right]_{\Gamma} = \sigma \kappa \quad (5)$$

$$[\mu \nabla \mathbf{u}]_{\Gamma} = [\mu]_{\Gamma} (\nabla \mathbf{u}) \begin{pmatrix} 0 \\ \mathbf{t} \end{pmatrix} \begin{pmatrix} 0 \\ \mathbf{t} \end{pmatrix}^T + [\mu]_{\Gamma} \mathbf{n}^T \mathbf{n} (\nabla \mathbf{u}) \mathbf{n}^T \mathbf{n} - \begin{pmatrix} 0 \\ \mathbf{t} \end{pmatrix} \begin{pmatrix} 0 \\ \mathbf{t} \end{pmatrix}^T [\mu]_{\Gamma} (\nabla \mathbf{u})^T \cdot \mathbf{n}^T \mathbf{n} \quad (6)$$

In Eq. (5)  $\sigma$  is surface tension. This equation represents the pressure jump at the interface. In addition, Eq. (6) expresses the jump condition at the interface, which must be applied when viscous terms are calculated.

## 3. NUMERICAL METHODS

Governing equations are discretized on a staggered grid by using the finite difference method. The projection method (Kang *et al.*, 2000) is employed to solve flow equations. The level-set method along with the ghost fluid method is utilized to model the interface in a sharp fashion. Temporal terms are discretized by using the third order TVD Runge-Kutta method (Kang *et al.*, 2000). The fifth order WENO scheme (Fedkiw *et al.*, 1999) and second order central approximation are used for the discretization of convection and diffusion terms, respectively.

### 3.1 Level-Set Method

In this method, computational domain  $\Omega$  is divided into three regions (as it is observed in Fig. 2) by the definition of a scalar function  $\phi$  (level-set function) as a signed distance function. This function is zero at the interface and is positive in one phase but negative in another phase (Pournaderi and Pischevar 2012; Shaobai *et al.* 2016).

Interface is considered as zero level set of function  $\phi$ . Thus, the governing equation can be expressed as,

$$\frac{\partial \phi}{\partial t} + \mathbf{u}_{\Gamma} \cdot \nabla \phi = 0 \quad (7)$$

where  $\mathbf{u}_{\Gamma}$  is the interface velocity. The zero level set of function  $\phi$  determines the location of the interface. Equation (7) implies that the zero level set of function  $\phi$  remains the zero level set of this function by advancing in time. The main use of Eq. (7) is at the interface. In this equation  $\mathbf{u}_{\Gamma}$  is the local fluid velocity at the interface. Although Eq. (7) is related to the interface, nevertheless it can be used for other regions of the computational domain. In this case, other level sets of function  $\phi$  remain also unchanged by advancing in time. In the current study, Eq. (7) is applied for all nodes of the domain including the nodes around the interface and the local velocity of each node is used in this equation instead of  $\mathbf{u}_{\Gamma}$ . By using this approach, the value of the level-set function is computed for each node at the new time. Thus, the new location of the interface (zero level set of  $\phi$ ) is also obtained. Since the level-set function is first defined as a

distance function, applying the level-set equation at all nodes of the domain results in its remaining as distance function in the next time step, at least theoretically. However, due to numerical errors, level-set function deviates from distance function by advancing in time. Therefore, level-set function must be reinitialized to preserve the accuracy of the method. Usually, the following equation is used for the reinitialization of the level- set function:

$$\frac{\partial \phi}{\partial \tau} = S(\phi_0)(1 - |\nabla \phi|) \quad (8)$$

where  $\tau$  is pseudo time.  $\phi_0$  represents level-set function values before reinitialization.  $S$  is a smeared out sign function:

$$S(\phi_0) = \frac{\phi_0}{\sqrt{\phi_0^2 + \varepsilon^2}} \quad (9)$$

where  $\varepsilon = \max(\Delta x, \Delta y)$ . When Eq. (8) is solved in the steady state, the distance function condition for  $\phi$  ( $|\nabla \phi| = 1$ ) is fulfilled. For positive values of the level-set function (gas phase),  $S(\phi_0)$  is positive and as a result Eq. (8) propagates information in the normal direction. Therefore, the direction of the information propagation is from smaller values of  $\phi$  to larger values of  $\phi$ . For negative values of the level-set function (liquid phase),  $S(\phi_0)$  is negative and Eq. (8) propagates information in the opposite direction. When a usual sign function is used in Eq. (8) (instead of a smeared-out sign function), accurate results are obtained as long as  $\phi$  is relatively smooth across the interface. If  $\phi$  is not smooth, the interface may be displaced incorrectly. Smeared-out distance function produces better results when  $\phi$  is not smooth.

Unit normal vector  $\mathbf{n}$  and curvature  $\kappa$  can be computed by using level-set function as:

$$\mathbf{n} = \begin{pmatrix} n_1 \\ n_2 \end{pmatrix} = \frac{\nabla \phi}{|\nabla \phi|} \quad (10)$$

$$\kappa = -\nabla \cdot \mathbf{n} \quad (11)$$

### 3.2 Contact Angle Models

Contact angle is applied during solution procedure by using the following equation (Malgarinos *et al.*, 2014):

$$\mathbf{n} = \cos(\theta)\mathbf{n}_w + \sin(\theta)\mathbf{t}_w \quad (12)$$

where  $\theta$  and  $\mathbf{n}$  are contact angle and unit normal vector at the interface, respectively.  $\mathbf{n}_w$  and  $\mathbf{t}_w$  represent unit normal vector to the wall and unit tangent vector to the wall, respectively. Using Eq. (10) and  $\mathbf{n}_w = (0, -1)^T$ , Eq. (12) can be rewritten as:

$$\phi_y = -\cos(\theta) \quad (13)$$

The distance function property ( $|\nabla \phi| = 1$ ) has been applied in the derivation of the above equation. Note that Eqs. (12) and (13) are only imposed on the solid wall.

The simplest model for contact angle is the static model. In this model, a constant angle (equilibrium angle) is considered as contact angle whereas in dynamic models, contact angle changes during impact process. Contrary to the static contact angle, dynamic contact angle is not a characteristic of the material. Many relations have been proposed for the computation of the dynamic contact angle based on the Capillary number and the velocity of the collision line. The velocity of the collision line is not the same as the material velocity and so cannot be easily extrapolated by using the velocity field. This velocity is computed as follows:

$$U_{cl} = \frac{dr}{dt} \quad (14)$$

where  $r$  is the radius of the wet region on the wall. One of the relations widely used in contact angle modeling is the Hoffman's law (Hoffman, 1974), which is used for small Capillary number flows,

$$\theta_d^3 - \theta_e^3 \cong c_T Ca \quad (15)$$

In the above equation,  $\theta_d$  and  $\theta_e$  are dynamic and equilibrium contact angle, respectively. In addition,  $Ca = \mu U_{cl} / \sigma$  is the Capillary number and  $c_T \approx 72$ .

Jiang *et al.* (1979) presented the following empirical correlation for dynamic contact angle:

$$\frac{\cos(\theta_e) - \cos(\theta_d)}{\cos(\theta_e) + 1} = \tanh(4.96Ca^{0.702}) \quad (16)$$

### 3.3 Ghost Fluid Method

The main idea of the ghost fluid method is the proper modeling of boundary conditions at the interface. Using this method, interface is modeled in a sharp fashion (Kang *et al.*, 2000; Liu *et al.*, 2000). To illustrate this method, consider the variable  $u$  that is discontinuous at the interface, as shown in Fig. 2. Suppose that  $[u]_r = a_r$ . For instance, the discretization of the simple equation  $\partial^2 u / \partial x^2 = 0$ , is explained. Proper discretization is carried out according to the interface location. When interface is located between  $x_i$  and  $x_{i+1}$ , the above equation is discretized at  $x_i$  and  $x_{i+1}$  in order, as follows:

$$\frac{u_{i+1}^g - u_i^-}{\Delta x} - \frac{u_i^- - u_{i-1}^-}{\Delta x} = 0 \quad (17)$$

$$\frac{u_{i+2}^+ - u_{i+1}^+}{\Delta x} - \frac{u_{i+1}^+ - u_i^g}{\Delta x} = 0 \quad (18)$$

The superscript + and - are used for velocities in

$\Omega^+$  and  $\Omega^-$  subdomains. The ghost values,  $u_i^{g+}$  and  $u_{i+1}^{g-}$ , are determined by using jump condition as:

$$u_i^{g+} = u_i^- + a_\Gamma \tag{19}$$

$$u_{i+1}^{g-} = u_{i+1}^+ - a_\Gamma \tag{20}$$

Using the above equations for ghost values, Eqs. (17) and (18) after omitting + and - superscripts can be rewritten as:

$$\frac{u_{i+1} - 2u_i + u_{i-1}}{\Delta x^2} = \frac{a_\Gamma}{\Delta x^2} \tag{21}$$

$$\frac{u_{i+2} - 2u_{i+1} + u_i}{\Delta x^2} = -\frac{a_\Gamma}{\Delta x^2} \tag{22}$$

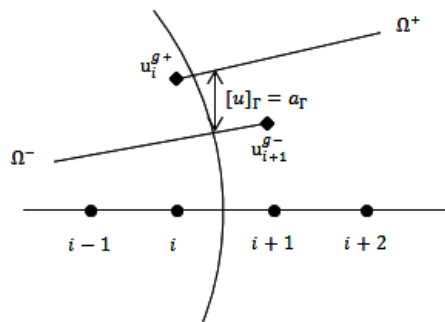


Fig. 2. Jump in a variable at interface.

#### 4. RESULTS

In this section, simulation results for droplet impact on a solid surface are presented. Figure 3 shows the computational domain and boundary conditions.  $D_0$  and  $V_0$  represent droplet diameter and impact velocity, respectively. According to the problem geometry, the governing equations are used in the axisymmetric form. Neumann boundary condition is applied on the symmetry boundary. Free boundary condition is used for the top and right boundaries. In addition, no slip condition is applied on the wall. The grid is considered uniform with a spacing of  $\Delta x = \Delta y = R_0/45$ .

##### 4.1 Grid Study

In this section, water droplet impact on a Teflon surface is simulated for different grid sizes by using the Hoffman's dynamic model. Computational domain size is  $4R_0 * 5R_0$ . Droplet impact velocity and static contact angle are 0.7m/s and  $110^\circ$ , respectively. Corresponding Weber and Reynolds numbers  $\left( We = \frac{\rho V_0^2 D_0}{\sigma}, Re = \frac{\rho V_0 D_0}{\mu} \right)$  for this simulation are 20 and 2100, respectively.

Figure 4 shows the spreading diameter of the droplet versus time for different grids. In the spreading stage, droplet diameter increases and at

the end of this stage, it reaches a maximum value. Then, in the recoiling stage, spreading diameter decreases. As could be seen, the difference between the results for the grid resolutions of  $R_0/45$  and  $R_0/90$  is negligible. The maximum difference between the two curves is less than 2 percent. Therefore, for the purpose of minimizing the computational cost, a grid with a resolution of  $R_0/45$  is used for all simulations.

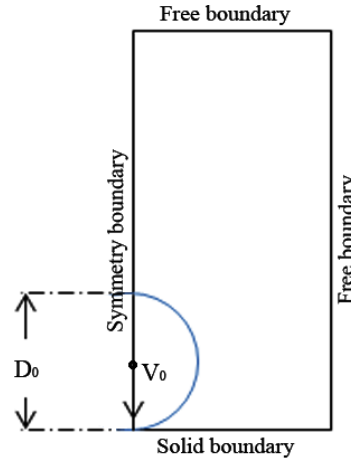


Fig. 3. Computational domain and boundary conditions.

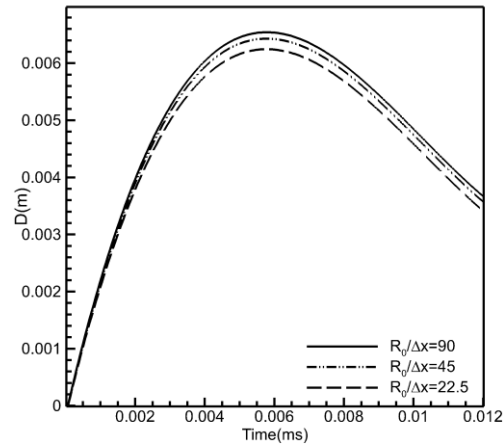
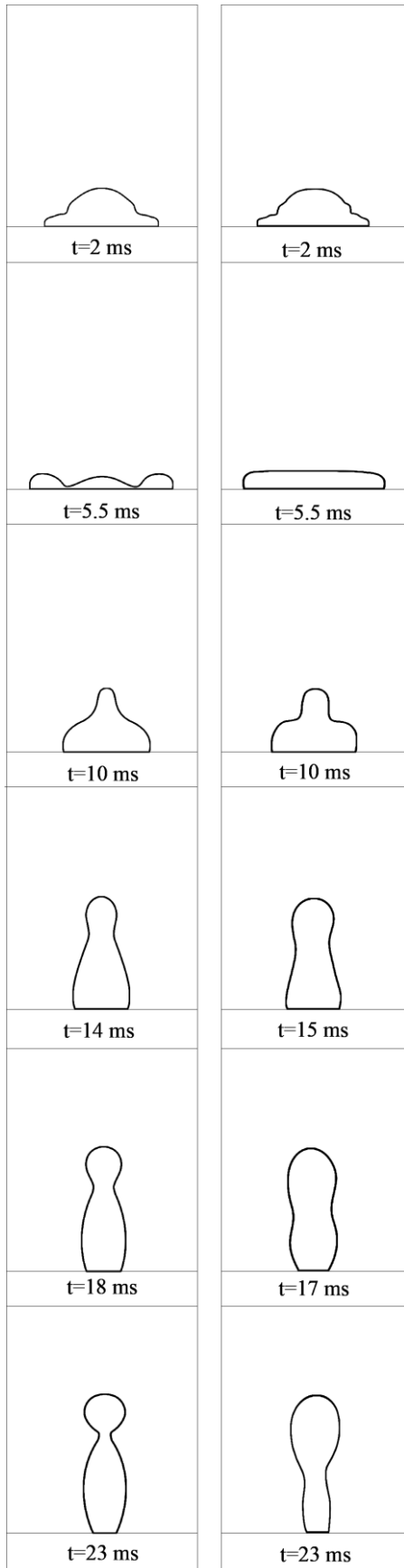


Fig. 4. Spreading diameter versus time for different grid resolutions based on the Hoffman's dynamic model  $V_0=0.7\text{m/s}$ ,  $We=20$ ,  $Re=2100$ .

##### 4.2 Validation of the Numerical Model

In this section, the validity of the numerical results for different contact line models is considered. Computational domain size is  $4R_0 * 8R_0$ . A water droplet impacts on a surface with a velocity of 0.7m/s ( $We = 20$ ,  $Re = 2100$ ). Figure 5 (left) represents the droplet profile at different stages of the impact process based on the Hoffman's dynamic model. Due to the inertia force, the droplet spreads on the surface. Viscous and surface tension forces resist against the droplet spreading. During the droplet spreading, surface tension resistant force



**Fig. 5. Droplet profile during the impact process. Left, numerical results (based on the Hoffman's model). Right, experimental results (Gatne, 2006). ( $V_0=0.7\text{m/s}$ ,  $We=20$ ,  $Re=2100$ ).**

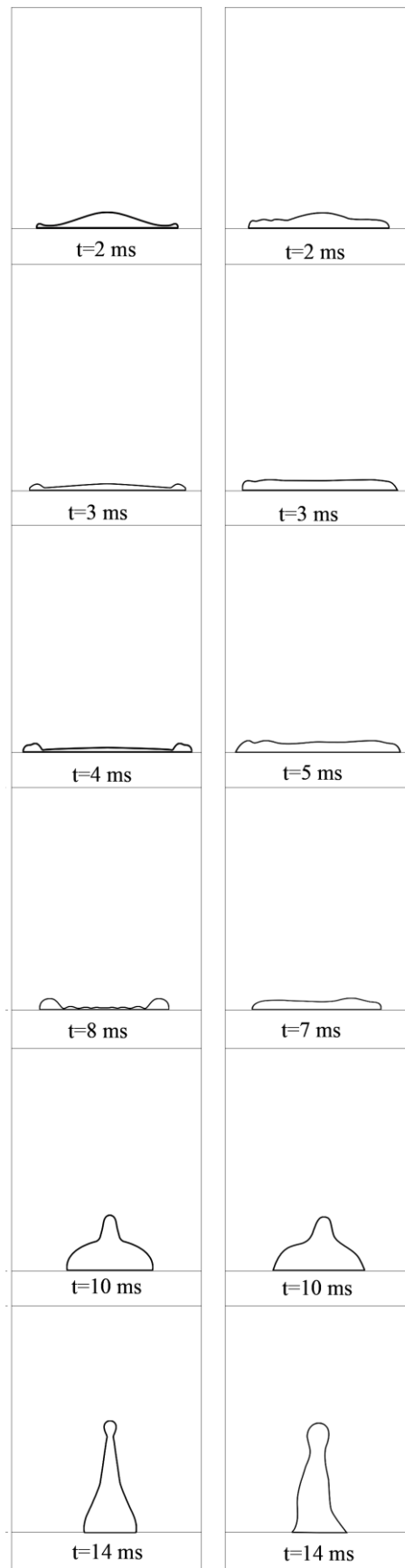


**Fig. 6. Droplet profile during the impact process. Left, numerical results (based on the Hoffman's model). Right, experimental results (Gatne, 2006). ( $V_0=1.39\text{m/s}$ ,  $We=80$ ,  $Re=4170$ ).**

increases due to the enhancement of the curvature of the droplet edge. The droplet reaches the maximum spreading radius at  $t=5.5m/s$ . At this moment, the surface tension force is dominant and as a result the droplet recoiling starts. At the end of the recoiling stage, the droplet tends to rebound from the surface due to its inertia. Figure 5 (right) represents the corresponding experimental results (Gatne, 2006). The comparison of numerical and experimental results indicates that the numerical procedure can successfully reproduce the droplet profile during the impact process. Note that the apparent difference between the results at  $t=5.5m/s$  is due to our axisymmetric solution procedure. For better comparative purposes, our result should be rotated about the symmetry axis. In fact, a dimple is formed in the center of the droplet.

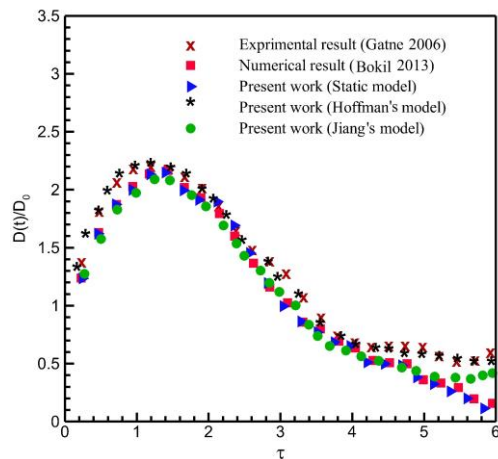


**Fig. 7. Time variations of the droplet spreading diameter for different models in comparison with the experimental (Gatne, 2006) and numerical results (Bokil, 2013). ( $V_0=0.7m/s$ ,  $We=20$ ,  $Re=2100$ ).**

To evaluate the capability of the numerical procedure at higher impact velocities, the impact process with a velocity of  $1.39m/s$  ( $We = 80$ ,  $Re = 4170$ ) is simulated. Figure 6 represents simulation (left) and experimental (right) results (Gatne, 2006). In this case, computational domain size is  $4R_0 * 9R_0$ . As it is observed, due to higher inertia, maximum spreading diameter of the droplet increases. In addition, in comparison to the previous case, the droplet requires less time to rebound from the surface. In the rebounding stage, inertia force overcomes the surface tension force and as a result, a small droplet is detached. As could be seen, the numerical procedure accurately predicts the droplet behavior during the impact process. At higher impact velocities, less time is required for the droplet to rebound from the surface.

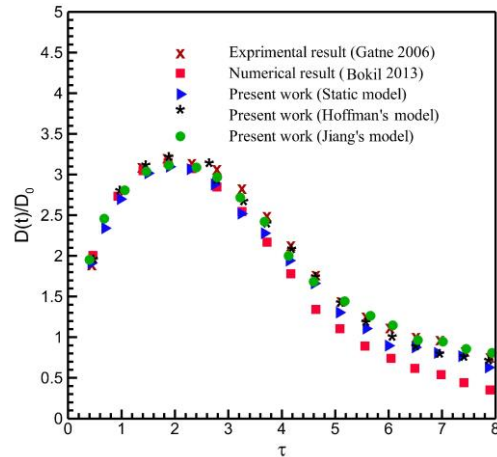


**Fig. 8. Time variations of the droplet spreading diameter for different models in comparison with the experimental (Gatne, 2006) and numerical results (Bokil, 2013). ( $V_0=1.39 m/s$ ,  $We=80$ ,  $Re=4170$ ).**

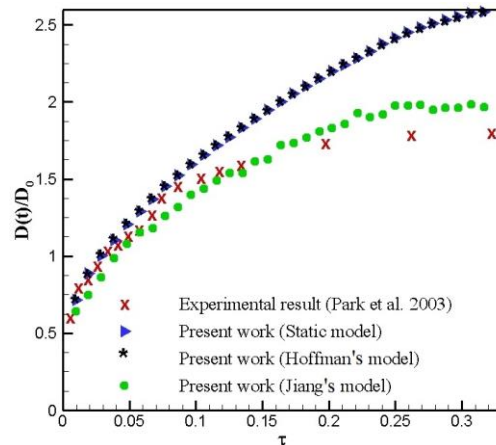


**Fig. 9. Time variations of the droplet spreading diameter for different models in comparison with the experimental results (Park et al., 2003). ( $V_0=0.08m/s$ ,  $We=0.2$ ,  $Re=184$ ).**

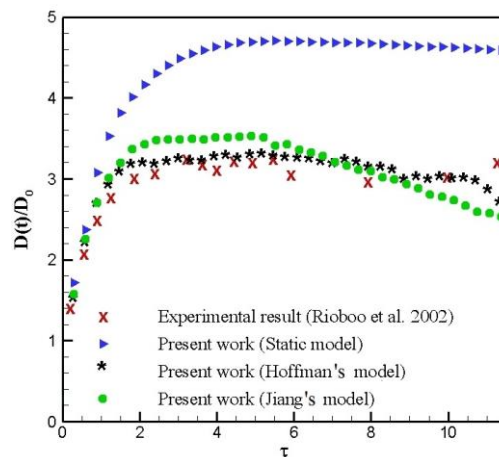


**Fig. 10. Time variations of the droplet spreading diameter for different models in comparison with the experimental results (Rioboo et al., 2002). ( $V_0=1.18 m/s$ ,  $We=59$ ,  $Re=3587$ ).**

Figures 7 and 8 represent time variations of droplet spreading diameter for impact velocities of 0.7m/s and 1.39m/s, respectively.  $\tau = tV_0/D_0$  is non-dimensional time. In these figures, the simulation results for different contact line models are compared against the experimental (Gatne, 2006) and the numerical (Bokil, 2013) results. Bokil (2013) simulated droplet impact by using the VOF method and based on the static and molecular kinetic dynamic models. According to the figures, the agreement between the simulation and the experiment is satisfactory. As the impact velocity increases, the maximum spreading radius of the droplet increases. In the spreading stage, the static model accurately predicts droplet spreading diameter. However, in a part of the recoiling stage and especially in the rebounding stage, Hoffman and Jiang's dynamic models represent more accurate prediction of the droplet spreading diameter than the static and molecular kinetic models. It could be seen that the molecular dynamic model is not appropriate for higher impact velocity. For the lower impact velocity, the Hoffman's model yields more accurate results whereas the Jiang's model is more appropriate for the higher impact velocity. Although our interface tracking method is different from the method used by Bokil *et al.*, the deviation of their results from the experiment is mainly due to their dynamic model. This is because they obtained satisfactory results based on the static model.

For further evaluation of different contact line models, water droplet collision with a hydrophilic surface (contact angle less than 90°) for two impact velocities is also simulated. In the first simulation, impact velocity and equilibrium contact angles are 0.08m/s ( $We = 0.2$ ,  $Re = 184$ ) and 31°, respectively. Figure 9 shows the time variations of the droplet spreading diameter for various contact line models, in comparison with the experimental results (Park *et al.*, 2003). As it is observed, the Jiang's model represents a satisfactory prediction of the spreading diameter whereas the static and the Hoffman's models are not able to produce accurate results, after initial stages of the impact process. In the next simulation, impact velocity is 1.18m/s ( $We = 59$ ,  $Re = 3587$ ). Advancing and receding contact angles are 10° and 6°, respectively. In our simulations, the average of these two angles was used as static contact angle. Figure 10 represents the droplet spreading diameter as a function of time. In this figure, numerical results for different contact line models are compared against the experimental results (Rioboo *et al.*, 2002). In this case, the values obtained from the static model show a large deviation from the experimental results. Dynamic models represent acceptable results. Especially the Hoffman's model shows considerable agreement with the experimental results almost throughout the entire impact process.

### 4.3 Contact Angle Effect

In this section, the effect of the contact angle on the hydrodynamic of the impact process is investigated

by using the Hoffman's dynamic model. Droplet diameter and impact velocity are 3 mm and 0.7m/s.

Figure 11 shows the simulation results for different contact angles. According to the results, the droplet spreading factor ( $D_{max} / D_0$ ) decreases with increases in the contact angle. This reduction can be observed in Fig. 12 in quantitative terms. It is concluded that the wettability of the surface decreases as the contact angle increases. For contact angles less than 90°, the inertia force overcomes the surface tension force and as a result, the droplet spreads on the surface and reaches the equilibrium state. However, for angles greater than 90°, the droplet reaches the maximum spreading radius and at this moment, due to the domination of the surface tension force, it starts to recoil. In this case, since the droplet has less contact with the surface, the effect of the viscose force is less. At the end of the recoiling stage, the droplet rebounds from the surface, which is due to its inertia. During the rebounding stage, a secondary droplet may form. At higher contact angles, it takes the droplet less time to rebound.

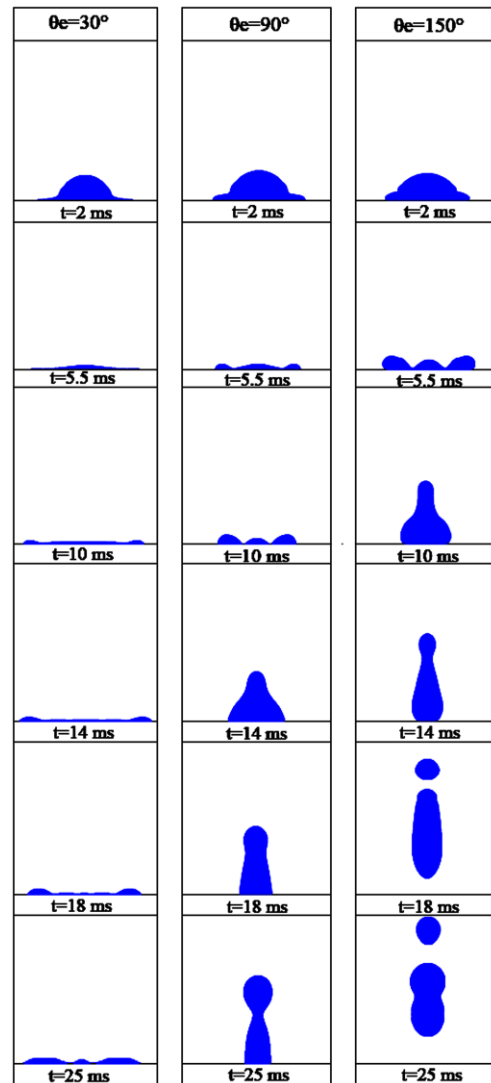


Fig. 11. Effect of the contact angle on the impact process ( $V_0=0.7m/s$ ,  $We=20$ ,  $Re=2100$ ).

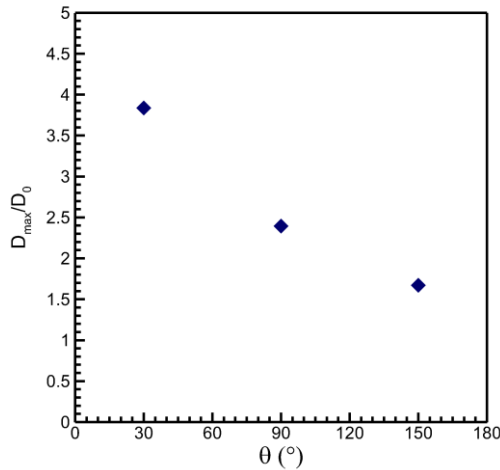


Fig. 12. Droplet spreading radius at different contact angles ( $V_0=0.7$  m/s,  $We=20$ ,  $Re=2100$ ).

## 5. CONCLUSION

In the present study, the droplet impact process on a wall is simulated by adopting a sharp approach for interface modeling. This approach is based on imposing appropriate jump conditions on the interface by using the level-set method along with the ghost fluid method. Hydrodynamic behavior of the droplet during the impact process for low and high Weber numbers is predicted successfully. Droplet impact velocities are in the range where droplet breakup does not occur. Several contact line models are compared and evaluated for different impact conditions. The effect of the contact angle on the impact process is considered. The main results can be summarized as follows:

1. For contact angles less than  $90^\circ$ , the droplet spreads on the surface and reaches an equilibrium state whereas for angles greater than  $90^\circ$ , after spreading and recoiling, the droplet may rebound from the surface. At higher impact velocities, it takes the droplet less time to rebound from the surface. The droplet maximum spreading radius decreases with increases in the contact angle. At higher contact angles, it takes the droplet less time to rebound from the surface.
2. On a hydrophobic surface, dynamic models developed by Hoffman and Jiang represent more accurate prediction of droplet spreading diameter than the static and molecular kinetic models.
3. Maximum spreading radius of droplet increases with an increase in the impact velocity. On a hydrophobic surface at low impact velocities, the Hoffman's model represents more accurate results whereas the Jiang's model is more appropriate for high impact velocities. The molecular dynamic model is not appropriate for high impact velocities. On a hydrophilic surface, at low impact velocities, the Jiang's model represents satisfactory results whereas the static and the Hoffman's models cannot

produce accurate results. For high impact velocities, the static model shows a great deviation from the experimental results. Dynamic models, especially the Hoffman's model, represent acceptable results.

## REFERENCES

- Afkhami, S. and M. Bussmann (2006). Drop impact simulation with a velocity-dependent contact angle. *19th Annual Conference on Liquid Atomization and Spray Systems*, Toronto, Canada.
- Afkhami, S., S. Zaleski and M. Bussmann (2009). A mesh-dependent model for applying dynamic contact angles to VOF simulations. *Journal of Computational Physics* 228, 5370-5389.
- Bokil, S. A. (2013). *On computational modeling of dynamic drop-surface interaction during post-impact spreading of water and aqueous surfactant solution*. MSc Thesis, University of Cincinnati, Cincinnati.
- Bussmann, M., S. Chandra and J. Mostaghimi (2000). Modeling the splash of a droplet impacting a solid surface. *Physics of Fluids* 12(12), 3121-3132.
- Cimpeanu, R. and D. T. Papageorgiou (2018). Three-dimensional high speed drop impact onto solid surfaces at arbitrary angles. *International Journal of Multiphase Flow* 107, 192-207.
- Fedkiw, R. P., T. B. Aslam, B. Merriman and S. Osher (1999). A non-oscillatory Eulerian approach to interfaces in multimaterial flows (the ghost fluid method). *Journal of Computational Physics* 152, 457-492.
- Fujimoto, H., Y. Shiotani, A. Y. Tong, T. Hama and H. Takuda (2007). Three-dimensional numerical analysis of the deformation behavior of droplets impinging onto a solid substrate. *International Journal of Multiphase Flow* 33(3), 317-332.
- Gatne, K. P. (2006). *Experimental investigation of droplet impact dynamics on solid surfaces*. PhD Thesis, University of Cincinnati, Cincinnati.
- Griebel, M. and M. Klits (2014). Simulation of droplet impact with dynamic contact angle boundary conditions. In: *Griebel M. (eds) Singular phenomena and scaling in mathematical models*. Springer, Cham.
- Guo, Y., Y. Lian and M. Sussman (2016). Investigation of drop impact on dry and wet surfaces with consideration of surrounding air. *Physics of Fluids* 28, 073303.
- Harlow, F. H. and J. P. Shannon (1967). The splash of a liquid drop. *Applied Physics Letters* 38, 3855.
- Hoffman, R. L. (1974). A study of the advancing

- interface. I. Interface shape in liquid-gas systems. *Journal of Colloid and Interface Science* 50, 228-241.
- Hu, J., R. Jio, X. Huang, X. Xiong and K. Wan (2015). Numerical simulation of the dynamics of water droplet impingement on a wax surface. *ASEE Northeast Section Conference*.
- Jiang, T. S., O. Soo-Gun and J. C. Slattery (1979). Correlation for dynamic contact angle. *Journal of Colloid and Interface Science* 69(1), 74-77.
- Kang, M., R. P. Fedkiw and X. D. Liu (2000). A boundary condition capturing method for multiphase incompressible flow. *Journal of Scientific Computing* 21, 323-369.
- Kim, H. Y. and J. H. Chun (2001). The recoiling of liquid droplets upon collision with solid surfaces. *Physics of Fluids* 13, 643.
- Kistler, S. F. (1993). Hydrodynamics of wetting. *Wettability* 6, 311-430.
- Li, S., Z. Yan, R. Li, L. Wang and J. Luan (2016). Numerical simulation of single bubble rising in shear-thinning fluids by level set method. *Journal of Central South University* 23, 1000-1006.
- Liu, H., S. Krishnan, S. Marella and H. S. Udaykumar (2005). Sharp interface Cartesian grid method II: A technique for simulating droplet interactions with surfaces of arbitrary shape. *Journal of Computational Physics* 210, 32-54.
- Liu, X. D., R. P. Fedkiw and M. Kang (2000). A boundary condition capturing method for Poisson's equation on irregular domains. *Journal of Computational Physics* 160, 151-178.
- Lunkad, S. F., V. V. Buwa and K. D. P. Nigam (2007). Numerical simulations of drop impact and spreading on horizontal and inclined surfaces. *Chemical Engineering Science* 62, 7214-7224.
- Luo, J., X. Y. Hu and N. A. Adams (2015). A conservative sharp interface method for incompressible multiphase flows. *Journal of Computational Physics* 284, 547-565.
- Luo, J., X. Y. Hu and N. A. Adams (2016). Curvature boundary condition for a moving contact line. *Journal of Computational Physics* 310, 329-341.
- Margarinos, I., N. Nikolopoulos, M. Marengo, C. Antonini and M. Gavaises (2014). VOF simulations of the contact angle dynamics during the drop spreading: standard models and new wetting force model. *Advances in Colloid and Interface Science* 212, 1-20.
- Muradoglu, M. and M. Tasoglu (2010). A front-tracking method for computational modeling of impact and spreading of viscous droplets on solid walls. *Computers & Fluids* 39(4), 615-625.
- Park, H. and W. W. Carr (2003). Single drop impaction on a solid surface. *AIChE Journal* 49(10), 2461-2471.
- Pasandideh-Fard, M., Y. M. Qiao, S. Chandra and J. Mostaghimi (1996). Capillary effects during droplet impact on a solid surface. *Physics of Fluids* 8, 650.
- Pournaderi, P. and A. R. Pischevar (2012). A Numerical investigation of droplet impact on a heated wall in the film boiling regime. *Heat and Mass Transfer* 48, 1525-1538.
- Raman, K. A., R. K. Jaiman, T. Lee and H. Low (2016). Lattice Boltzmann simulations of droplet impact onto surfaces with varying wettabilities. *International Journal of Heat and Mass Transfer* 95, 336-354.
- Rioboo, R., M. Marengo and C. Tropea (2002). Time evolution of liquid drop impact onto solid, dry surfaces. *Experiments in Fluids* 33, 112-124.
- Roisman, I. V., L. Opfer, C. Tropea, M. Raessi, J. Mostaghimi and S. Chandra (2008). Drop impact onto a dry surface: role of the dynamic contact angle. *Colloids and Surfaces A: Physicochemical and Engineering Aspects* 322(1), 183-191.
- Shikhmurzaev, Y. D. (2008). *Capillary flows with forming interfaces*. Chapman & Hall/CRC, Boca Raton.
- Sikalo, S. and E. N. Ganic (2006). Phenomena of droplet-surface interactions. *Experimental Thermal and Fluid Science* 97-110.
- Sprittles, J. E. and Y. D. Shikhmurzaev (2012). The dynamics of liquid drops and their interaction with solids of varying wettabilities. *Physics of Fluids* 24, 082001.
- Tsurutani, K., M. Yao, J. Senda and H. Fujimoto (1990). Numerical analysis of the deformation process of a droplet impinging upon a wall. *JSME International Journal* 3, 555-561.
- Vontas, K., M. Andreadaki, A. Georgoulas, K. S. Nikas and M. Marengo (2017). Numerical investigation of droplet impact on smooth surfaces with different wettability characteristics: Implementation of a dynamic contact angle treatment in OpenFOAM. *28th Conference on Liquid Atomization and Spray Systems*, Valencia, Spain.
- Worthington, A. M. (1877). On the forms assumed by drops of liquids falling vertically on a horizontal plate. *Proceedings of the royal society of London* 25, 261-272.
- Yokoi, K., D. Vadiello, J. Hinch and L. Hutchings (2009). Numerical studies of the influence of the dynamic contact angle on a droplet impacting on a dry surface. *Physics of Fluids*

M. Emdadi and P. Pournaderi / *JAFM*, Vol. 12, No. 4, pp. 1001-1012, 2019.

21, 072102.

Zhang, Q., T. Z. Qian and X. P. Wang (2016).  
Phase field simulation of a droplet impacting  
a solid surface. *Physics of Fluids* 28, 02210.

Zisman, W. A. (1964). Relation of the Equilibrium  
Contact Angle to Liquid and Solid  
Constitution. *American Chemical Society*  
43,1-51.